RESEARCH PAPER

Anionic and Cationic Surfactants in Ammonia Gas-Mediated Synthesis of β-Ni(OH)$_2$ and NiO Nanostructures

Mohammadreza Mansournia* and Elham Moradinia

Department of Inorganic Chemistry, Faculty of Chemistry, University of Kashan, Kashan, Iran

ARTICLE INFO

ABSTRACT

Up to now, researchers have proposed several synthesis methods for the preparation of β-nickel(II) hydroxide nanostructures. Most of these approaches contain harsh synthetic conditions such as multi-step processes, high temperatures and long reaction time. In this work, a novel, facile and low cost method is introduced to produce of β-Ni(OH)$_2$ nanostructures using the gas-solution precipitation from nickel(II) sulfate solution in the presence of anionic or cationic surfactant upon exposure to ammonia gas at room temperature. Herein, no other additive is needed and the method is suited for large-scale preparation. The structural characterizations were carefully investigated by the powder X-ray diffraction technique and Fourier transformation infrared spectroscopy. Further, the scanning electron microscopy results showed the important roles of the sodium dodecylsulfate and cetyltrimethylammonium bromide on the morphology and size of the products. The calcination process of hydroxide samples was also conducted to synthesize nickel(II) oxide nanostructures.

How to cite this article

INTRODUCTION

Nickel(II) hydroxide and Nickel(II) oxide have been extensively studied due to theirs many significant applications. Ni(OH)$_2$ presents two polymorphs, α-Ni(OH)$_2$ and β-Ni(OH)$_2$ and plays important roles as the active material in the positive electrode of many rechargeable alkaline battery systems [1-3], and as the most common precursor for nickel oxides [4-6] and nickel catalysts [7-9]. Nickel(II) oxide (NiO) is a very interesting semiconductor material which widely used in catalysis [10], gas sensors [11], battery cathodes [12], magnetic materials [13], electrochromic devices [14], optical materials [15], and dye-sensitized solar cells [16].

The most common methods for preparing Ni(OH)$_2$ involve either chemical precipitation from nickel(II) salts, microemulsion and hydrothermal synthesis. The chemical precipitation method is extensively used in the industry, in which nickel(II) hydroxide is usually prepared from NiSO$_4$ solution, because the sulfate ions facilitate precipitation and decrease the absorbed impurities on the surface of Ni(OH)$_2$ particles [3,17-20]. Also, many methods for the synthesis of nickel(II) oxide have been reported, such as precipitation [21], microemulsion [22] and sol-gel [23].

Nanostructured materials display more attractive physical and chemical properties than conventional bulk materials, due to their quantum size effect, large surface to volume ratio, and high surface energy [22]. Accordingly, many reports are concerned with the synthesis of Ni(OH)$_2$ and NiO nanostructures with different morphologies, including nanoplates [24], nanoparticles [22,23,25], nanosheets [26-28], nanorods [29], nanowires [30] and nanoflakes

* Corresponding Author Email: Mansournia@kashanu.ac.ir

[27,31]. The objective of this work was to present the new and simple surfactant-assisted method for the synthesis of nickel(II) hydroxide nanostructures and their thermal decomposition to nanosized NiO.

MATERIALS AND METHODS

Nickel(II) sulfate hexahydrate, SDS, CTAB, ammonia solution (25%) and absolute ethanol were purchased from Merck company and used as received. The ammonia solution was standardized by acid-base titration before the preparation of 5 M NH_3 solution.

Synthesis of β-Ni(OH)₂ and NiO nanostructures

For the synthesis of $Ni(OH)_2$ nanostructures, a 50 mL aqueous solution of $NiSO_4.6H_2O$ (0.01 M) and surfactant (0.01 or 0.001 M) was stirred for 15 min and then put into a sealed glass container which included 25 mL 5 M solution of NH_3. The container had a capacity of about 1000 mL. The solution of Ni(II) salt and surfactant was kept under ammonia atmosphere for 30 min at room temperature and was stirred continuously all the while. The green precipitate was separated by centrifuge and rinsed with distilled water and ethanol several times, respectively, to remove the adsorbed ions, and then dried at 75 °C for 12 h. The as-made $Ni(OH)_2$ samples, denoted as SDS-0.01, SDS-0.001, CTAB-0.01 and CTAB-0.001 according to the applied surfactant and its concentration, were calcined at 300 °C in air for 2 h to obtain black NiO nanostructures.

Characterization techniques

The powder X-ray diffraction (XRD) patterns were made on a Phillips X'Pert Pro X-ray diffractometer with a Cu Kα (λ = 1.5418 Å) source. Crystallite size was evaluated by applying Scherrer's formula. Fourier transform infrared spectra (FT-IR) were recorded with the KBr pellet technique in the range of 4000-400 cm^{-1} on a Nicolet Magna 550 spectroscope. Morphological studies of the synthesized samples were carried out directly by a Hitachi S4160 field emission scanning electron microscope (15 kV). The particle size distribution of the products was measured by the diameter of about 100 particles on the magnified SEM images using Digimizer software.

RESULTS AND DISCUSSION

Noted, additive molecules such as surfactant could induce a template effect and lead to original and well-controlled morphologies. Herein, we used anionic and cationic surfactants for controlling size, shape, and crystallinity of the product. The comparison of typical XRD patterns (10° < 2θ < 80°) of the samples prepared using sodium dodecylsulfate and cetyltrimethylammonium bromide and their calcined products are shown in Figs. 1 and 2. The XRD patterns for the samples SDS-0.01 and SDS-0.001 (Figs. 1a and 1b, respectively) are in good agreement with a hexagonal phase of β-nickel(II) hydroxide with the space group of P-3m1, JCPDS card no. 01-1047. The broad reflection peaks observed in these two plots indicate fine particle nature of the obtained nanostructures. These peaks can be indexed as (001), (100), (101), (102), (110), (111), (200) and (112) crystal planes in the order of increasing 2θ. No additional diffraction peaks arising from other crystalline phases of $Ni(OH)_2$ were detected for these products. Further, from peak position (θ, in radian), full width at half maximum of the major diffraction peak (β), and the wavelength of the X-ray radiation (λ = 0.15418 nm), the crystallite size (D) of the products was calculated by Scherrer equation:

$$D = \frac{0.9\,\lambda}{\beta \cos\theta} \tag{1}$$

On this basis, the average crystallite size was estimated about 8 and 23 nm for SDS-0.01 and SDS-0.001, respectively. On the other hand, the X-ray diffraction pattern of SDS-0.01 sample after calcination in air at 300 °C for 2 h is presented in Fig. 1c. The reflections observed at about 2θ = 36.62, 43.18, and 62.22 were satisfactorily indexed to the (111), (200), and (220) crystal planes, respectively, from a cubic NiO with the space group Fm3m, according to JCPDS card no. 04-0835. No characteristic peaks of β-Ni(OH)₂ are detected, suggesting that the hydroxide precursor is completely converted to nickel oxide during calcination. From XRD data (Fig. 1c), the average crystallite diameter (D) of the as-prepared NiO was estimated to be 8 nm from the Scherrer equation.

Fig. 2a shows the X-ray diffraction pattern of the nickel(II) hydroxide derived from 0.01 M $NiSO_4$, 0.01 M CTAB, and 5 M NH_3 at 30 min (CTAB-0.01). All of the diffraction lines matched with (001), (100), (101), (102), (110), (111), (200), (103), and (201) planes are assigned to the hexagonal β-Ni(OH)₂ structure (JCPDS card no. 03-0177 with the space group P-3m1). The sharpness of the diffraction peaks is indicative of the high crystallinity of the synthesized $Ni(OH)_2$.
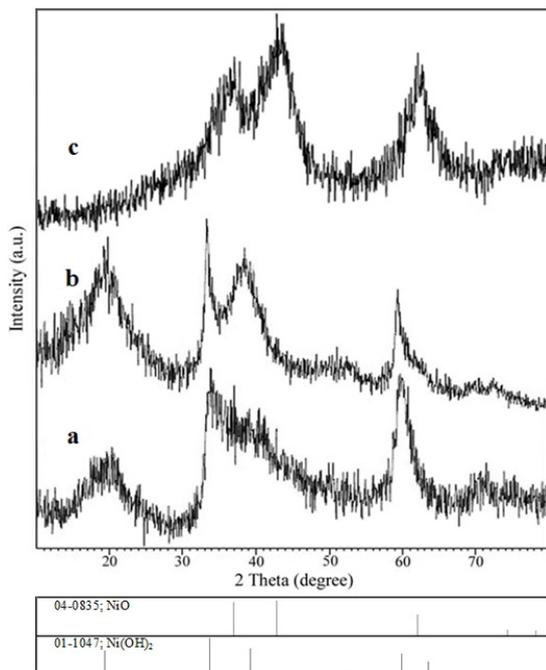
Fig. 1. XRD patterns of the as-synthesized β-Ni(OH)$_2$ and NiO: (a) SDS-0.01 and (b) SDS-0.001, and (c) SDS-0.01 after calcination

The XRD pattern of the calcined product of CTAB-0.01 is presented in Fig. 2b. The Bragg's reflections observed at 2θ values 36.65, 42.74, and 62.09 representing (111), (200), and (220) planes of cubic lattice of CuO, respectively, are in agreement with the literature value of JCPDS card No. 04-0835 (space group: Fm3m). Based on the XRD data, the crystallite diameter (D) of CTAB-0.01 and

its calcined product were calculated to be about 10 and 6 nm, respectively, using the Scherrere equation.

Besides further support the XRD results, infrared spectroscopy enables the molecules and ions either adsorbed on the surface or inserted in the interlayer space to be identified. The spectra of typical Ni(OH)$_2$, SDS-0.01 and CTAB-0.01, and their calcined products are shown in Fig 3. All samples indicate a broad and intense band centered at 3420-3450 cm^{-1}, corresponded to the O-H stretching vibration of interlayer water molecules and H-bound hydroxy groups, and the absorption band at around 1620-1630 cm^{-1} which can be assigned to the bending vibrational mode of H$_2$O molecules. They also reveal the presence of free sulfate anions whose v$_3$ and v$_4$ vibrational modes are positioned at 1116-1121 and 600-624 cm^{-1}, respectively.

As seen in Fig. 3b (CTAB-0.01), the strong and narrow absorption band located at 3641 cm^{-1} can be ascribed to OH stretching vibration, which is the typical IR characteristic of free OH groups in the brucite-like structure of β-Ni(OH)$_2$, whereas this peak is not observed for SDS-0.01 (Fig. 3a), because all the OH groups are available by water molecules. Moreover, The bands observed at ca. 480 and 515 cm^{-1} in plots 3a and 3b can result from Ni-OH stretching and Ni-O-H bending vibration modes. Furthermore, the stretching vibration of Ni-O bond for the calcined samples (spectra 3c and 3d) is observed at about 417 cm^{-1}.
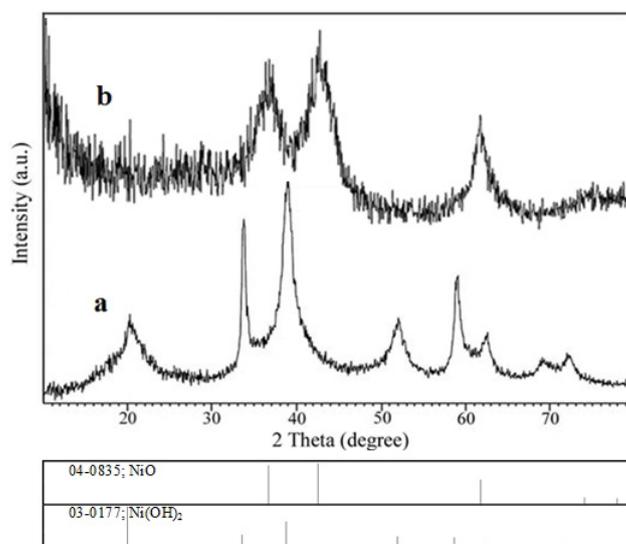

Fig. 2. XRD patterns of as-prepared samples: (a) CTAB-0.01 and (b) its calcined product
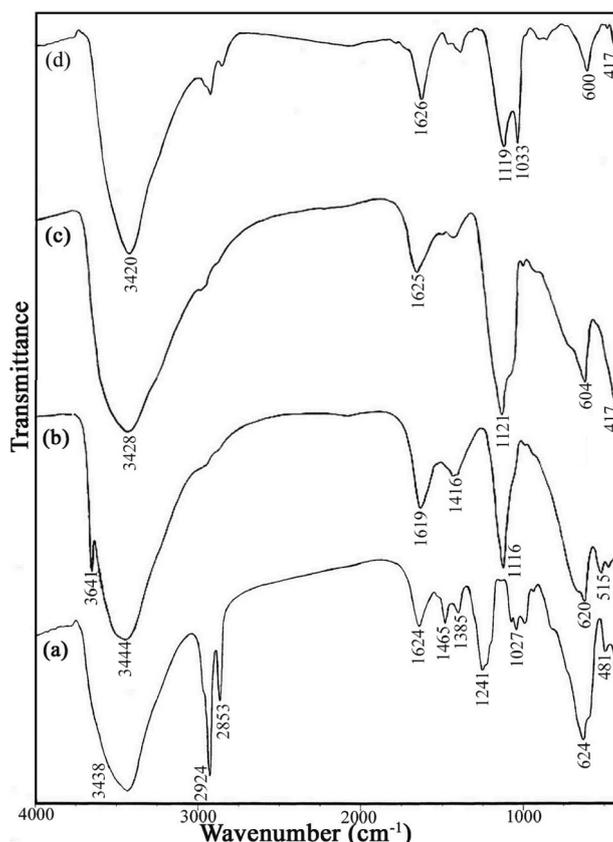
Fig. 3. FT-IR spectra of the typical samples before and after calcination: (a, c) SDS-0.01 and (b, d) CTAB-0.01.

In spectrum of SDS-0.01 (Fig. 3a), the bands at 2924 and 2853 cm^{-1} are due to the asymmetric and symmetric stretching vibrations of CH$_2$ groups, the band at 1465 cm^{-1} is related to their bending vibrations, and the absorption peaks located at 1241 cm^{-1} and in the range of 980-1080 cm^{-1} corresponds to the asymmetric and symmetric stretching modes of OSO$_3^-$, respectively, which prove the presence of DS^{-1}, probably intercalated in the interlayer galleries or not completely eliminated during the washing stage. Also, the band at about 1385 cm^{-1} can be assigned as C=O vibration of the adsorbed CO$_2$ molecules [25,32-36].

To investigate the overall morphology and size of the products obtained via the ammonia-assisted method using NiSO$_4$ 0.01 M with the aid of different concentrations of SDS and CTAB, they were characterized by SEM images, presented in Figs. 4-6. Furthermore, the insets in these figures show the particle size distribution of the as-synthesized Ni(OH)$_2$ and NiO nanostructures. The comparison of the SEM images of β-Ni(OH)$_2$ samples prepared in the presence of 0.01 and

0.001M of SDS at 30 min (Figs. 4a and 4b, respectively) indicates that in the case of 0.001 M surfactant (SDS-0.001), the curved nanoplates are more detectable, whose average thickness is in the range of 35-45 nm (according to inset of Fig. 4b). It seems that on increasing concentration of SDS (0.01 M), nucleation occurs more. Indeed, dodecylsulfate anions restrict the growth of nanostructures efficiently.

As shown in Fig. 5, the spherical-shape nanostructures of nickel(II) hydroxide organized from the nanoparticles with average particle diameter of 15-20 nm are obtained in the presence of CTAB, in both concentrations (0.01 and 0.001 M) which proves that the concentration of CTAB has no special effect on the morphology and size. In this specific applied method, the ammonia molecules slowly enter to the solution mixture of Ni^{2+} and surfactant, and are gradually converted to OH$^-$ anions through the basic dissolution equation 2, followed by reaction 3 to form Ni(OH)$_2$; therefore the concentration of cationic surfactant (cetyltrimethylammonium ion) don't have important
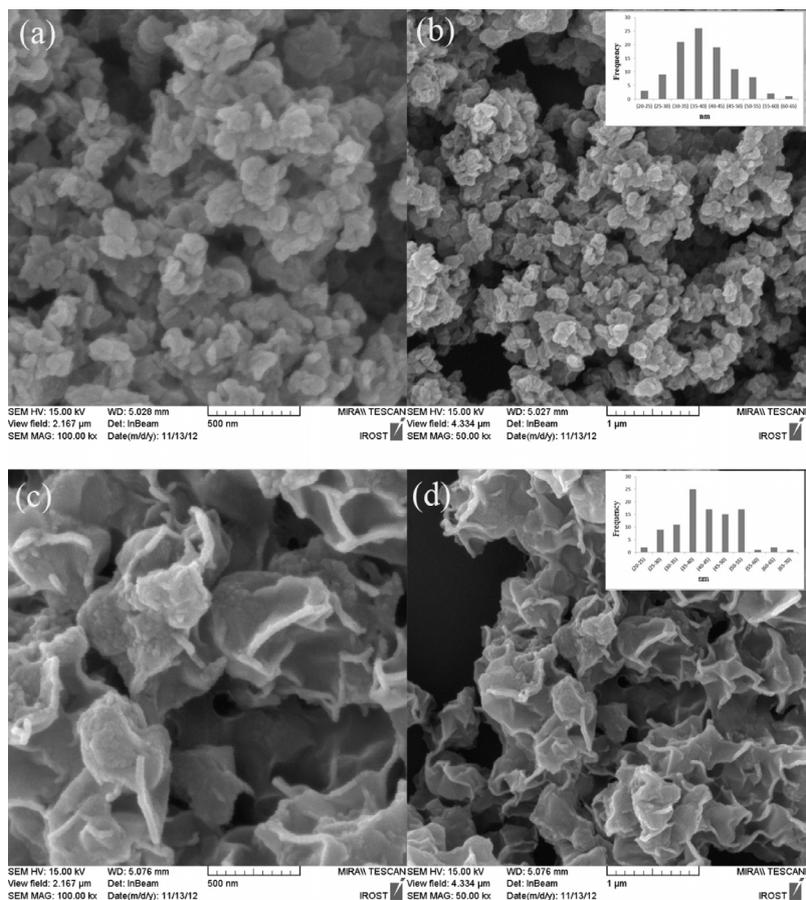
Fig. 4. SEM images of β-Ni(OH)$_2$ nanostructures prepared in the present of SDS: (a, b) SDS-0.01 and (c, d) SDS-0.001. The insets are the size distribution histograms.
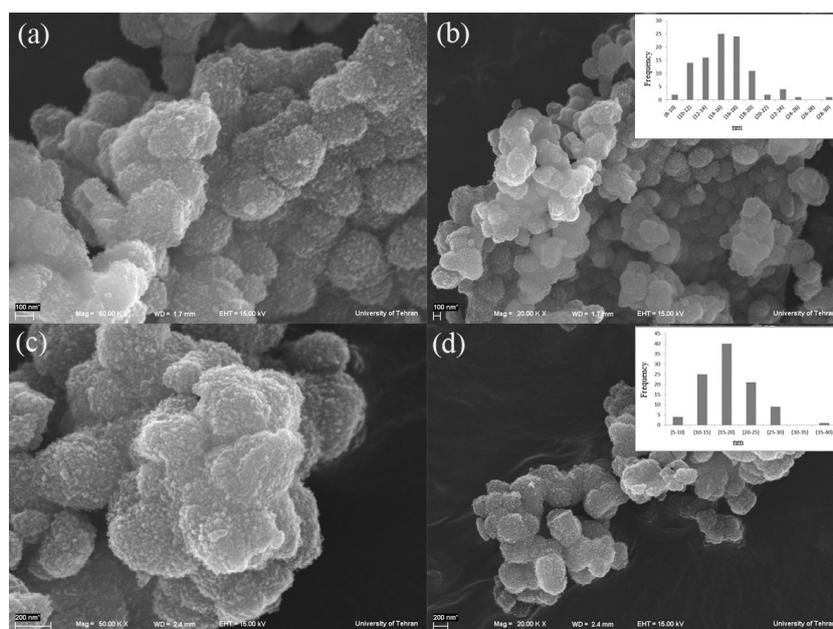

Fig. 5. SEM images of β-Ni(OH)$_2$ nanostructures in the present of CTAB: (a, b) CTAB-0.01 and (c, d) CTAB-0.001. The insets are the size distribution histograms.
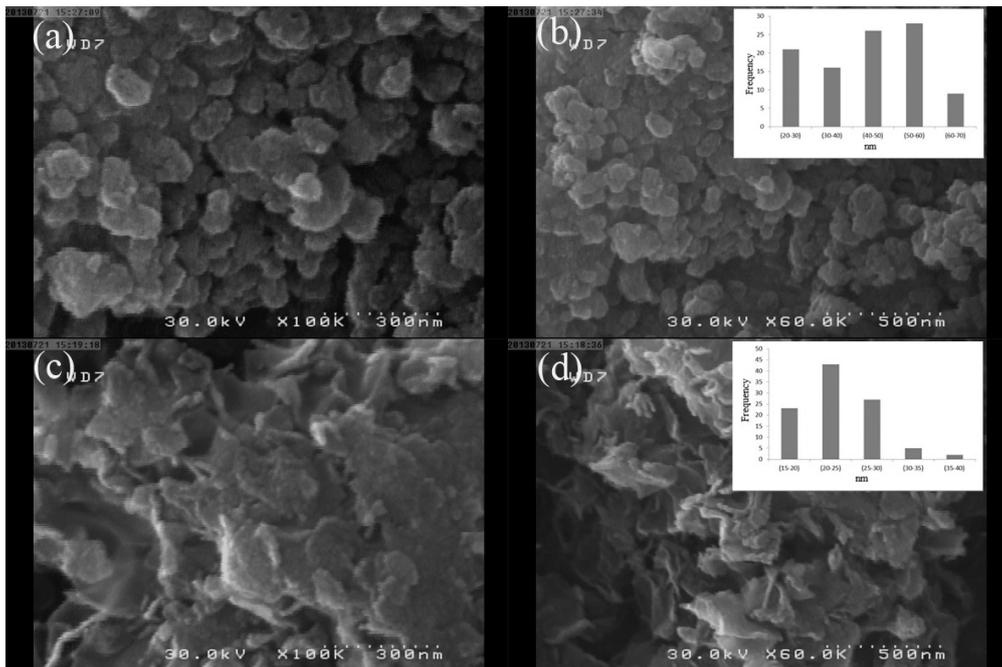
Fig. 6. SEM images of NiO nanostructures: (a, b) SDS-0.01 and (c, d) CTAB-0.01 samples after calcination. The insets are the size distribution histograms.
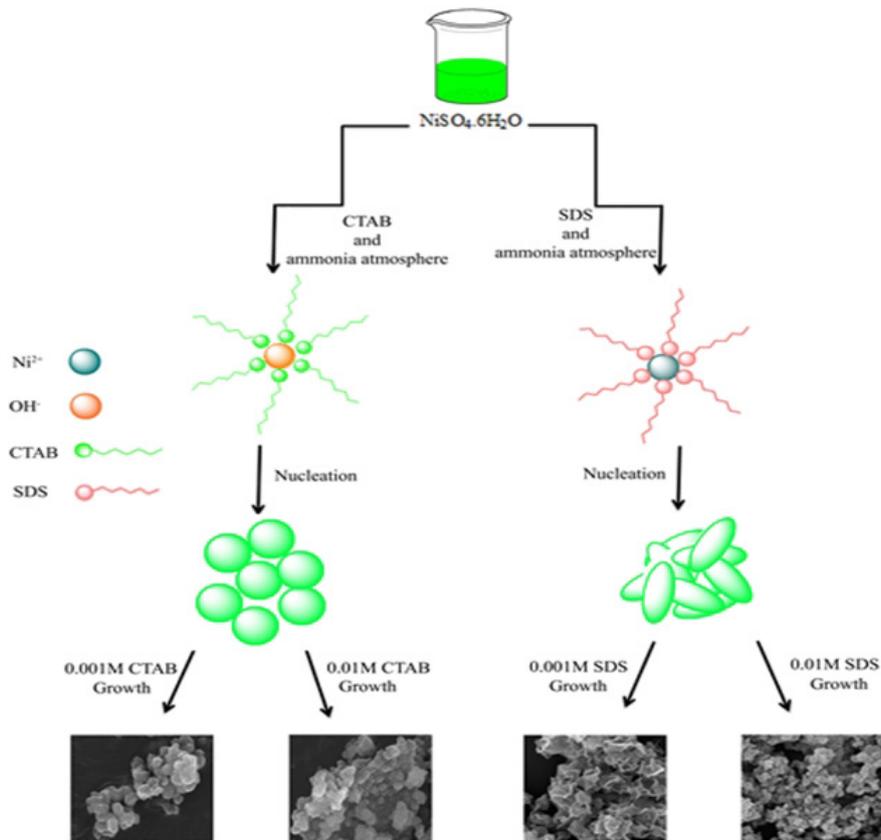

Fig. 7. Schematic diagram illustrating the formation of β-Ni(OH)$_2$ nanostructures with various morphology.

role in controlling the nucleation and growth rates. According to these observations, the possible mechanism process for the preparation of Ni(OH)$_2$ nanostructures has been shown in Fig. 7.

$$NH_3 + H_2O \rightarrow NH_4^+ + OH^- \qquad (2)$$

$$Ni^{2+} + 2OH^- \rightarrow Ni(OH)_2 \qquad (3)$$

On the other hand, the typical SEM pictures of NiO nanostructures obtained by calcination of nickel(II) hydroxide samples (SDS-0.01 and CTAB-0.01) are shown in Figs. 6a and 6b, respectively. The evaluation of these images in compared with those of hydroxide precursors indicates that there is morphological similarity between SDS-0.01 and its calcined product, whereas the NiO sample prepared in the presence of CTAB has different morphology than the prototype. However, it is observed that the particle sizes possess a narrow distribution for all samples.

CONCLUSIONS

The nickel(II) hydroxide nanostructures have been successfully synthesized by a simple gas-solution precipitation method in the presence of anionic and cationic surfactants. Then, the nickel(II) oxide nanostructures have been obtained from the Ni(OH)$_2$ samples by calcination at 300 °C. It was observed that the particle sizes possess a narrow distribution. Moreover, the surfactants play an important role in the growth process and effect as the directing agents to control the morphology and size of nanostructures. Compared with some relevant investigations on the synthesis of Ni(OH)$_2$ nanostructures, represented in Table 1, the method reported in this paper has several advantages, namely, mild reaction conditions such as synthesis at room temperature, simple production process, no need for organic solvent, low cost, and environmentally friendly procedure.

ACKNOWLEDGMENTS

CONFLICT OF INTEREST

The authors declare that there are no conflicts of interest regarding the publication of this manuscript.

REFERENCES

1. M.R. Palacin, Recent advances in rechargeable battery materials: a chemist's perspective, Chem. Soc. Rev. 2002; 38(9): 2565–2575.

2. H. Wang, H.S. Casalongue, Y. Liang, H. Dai, Ni(OH)₂ nanoplates grown on graphene as advanced electrochemical pseudocapacitor materials, J. Am. Chem. Soc. 2010; 132(21): 7472–7477.

3. J. Sun , J. Cheng , C. Wang , X. Ma , M. Li , L. Yuan, Synthesis and morphological control of nickel hydroxide for lithium-nickel composite oxide cathode materials by an Eddy circulating precipitation method, Ind. Eng. Chem. Res. 2006; 45(6): 2146–2149.

4. G.T. Zhou, Q.Z. Yao, X. Wang, J.C. Yu, Preparation and characterization of nanoplatelets of nickel hydroxide and nickel oxide, Mater. Chem. Phys. 2006; 98(2): 267–272.

5. J. Estellea, P. Salagre, Y. Cesteros, M. Serra, F. Medina, J.E. Sueiras, Comparative study of the morphology and surface properties of nickel oxide prepared from different precursors, Solid State Ionics. 2003; 156(1): 233–243.

6. A. Kalam, A.S. Al-Shihri, A.G. Al-Sehemi, N.S. Awwad, G. Du, T. Ahmad, Effect of pH on solvothermal synthesis of β-Ni(OH)₂ and NiO nano-architectures: surface area studies, optical properties and adsorption studies, Superlattices Microstruct. 2013; 55: 83–97.

7. Y. Wang, S. Gai, C. Li, F. He, M. Zhang, Y. Yan, P. Yang, Controlled synthesis and enhanced supercapacitor performance of uniform pompon-like β-Ni(OH)₂ hollow microspheres, Electrochim. Acta. 2013; 90: 673–681.

8. R. Gomez-Reynoso, J. Ramirez, R. Nares, R. Luna, F. Murrieta, Characterization and catalytic activity of Ni/SBA-15, synthesized by deposition–precipitation, Catal. Today. 2005; 107–108: 926–932.

9 G.W. Yang, C.L. Xu, H.L. Li, Electrodeposited nickel hydroxide on nickel foam with ultrahigh capacitance, Chem. Commun. 2008; 2(48): 6537–6539.

10. D. Wang, R. Xu, X. Wang, Y. Li, NiO nanorings and their unexpected catalytic property for CO oxidation, Nanotechnol. 2006 ;17(4): 979–983.

11. G. Mattei, P. Mazzoldi, M.L. Post, D. Buso, M. Guglielmi, A. Martucci, Cookie-like Au/NiO nanoparticles with optical gas-sensing properties, Adv. Mater. 2007 ;19(4): 561–564.

12. F.B. Zhang, Y.K. Zhou, H.L Li, Nanocrystalline NiO as an electrode material for electrochemical capacitor, Mater. Chem. Phys. 2004; 83(2): 260–264.

13. N.P. Duong, T. Satoh, M. Fiebig, Ultrafast manipulation of antiferromagnetism of NiO, Phys. Rev. Lett. 2004; 93(11): 117402–117404.

14. M.C.A Fantini, F.F Ferreira, A. Gorenste, Theoretical and experimental results on Au-NiO and Au-CoO electrochromic composite films, Solid State Ionics. 2002; 152–153: 867–872.

15. A.A. Al-Ghamdi, W.E. Mahmoud, S.J. Yaghmour, F.M. Al-Marzouki, Structure and optical properties of nanocrystalline NiO thin film synthesized by sol-gel spin-coating method, J. Alloys Compd. 2009; 486(1): 9–13.

16. A. Morandeira, J. Fortage, T. Edvinsson, L.L. Pleux ,E. Blart, G. Boschloo, A. Hagfeldt, L. Hammarström, F. Odobel, Improved photon-to-current conversion efficiency with a nanoporous p-type NiO electrode by the use of a sensitizer-acceptor dyad, J. Phys. Chem. C. 2008; 112(5): 1721–1728.

17. J.D.V. Rani, S. Kamatchi, A. Dhathathreyan, Nanoparticles of nickel oxide and nickel hydroxide using lyophilisomes of fibrinogen as template, J. Colloid Interface Sci. 2010 ; 341(1) 48–52.

18. L.X. Yang, Y.J. Zhu, H. Tong, Z.H. Liang, L. Li, L. Zhang,

Hydrothermal synthesis of nickel hydroxide nanostructures in mixed solvents of water and alcohol, J. Solid State Chem. 2007; 180(7): 2095–2101.

19. T. Neuberger, B. Schopf, H. Hofmann, M. Hofmann, B. von Rechenberg, Superparamagnetic nanoparticles for biomedical applications: possibilities and limitations of a new drug delivery system, J. Magn. Magn. Mater. 2005; 293(1): 483–496.

20. E. Zhang, Y. Tang, Y. Zhang, C. Guo, L. Yang, Hydrothermal synthesis of β-nickel hydroxide nanocrystalline thin film and growth of oriented carbon nanofibers, Mater. Res. Bull. 2009; 44(8): 1765–1770.

21. Z.M. Khoshhesab, M. Sarfaraz, Preparation and characterization of NiO nanoparticles by chemical precipitation method, Syn. React. Inorg. Met. Chem. 2010; 40(9): 700–703.

22. Y. Du, W. Wang, X. Li, J. Zhao, J. Ma, Y. Liu, G. Lu, Preparation of NiO nanoparticles in microemulsion and its gas sensing performance, Mater. Lett. 2012; 68: 168–170.

23. S. Thota, J. Kumar, Sol-gel synthesis and anomalous magnetic behavior of NiO nanoparticles, J. Phys. Chem. Solids. 2007; 68(10): 1951–1964.

24. H. Li, S. Liu, C. Huang, Z. Zhou, Y. Li, D. Fang, Characterization and supercapacitor application of coin-like β-nickel hydroxide nanoplates, Electrochim. Acta. 2011; 58: 89–94.

25. M. Aghazadeh, A.N. Golikand, M. Ghaemi, Synthesis, characterization, and electrochemical properties of ultrafine β-Ni(OH)$_2$ nanoparticles, J. Hydrogen Energy. 2011; 36(14): 8674–8679.

26. C. Guo , Y.H. Tang, E.L. Zhang , X.C. Li , J.L. Li, Aggregation of self-assembled Ni(OH)$_2$ nanosheets under hydrothermal conditions, J. Mater. Sci. Mater. Electron. 2009; 20(11): 1118–1122.

27. D. Wang , C. Song , Z. Hu , X. Fu, Fabrication of hollow spheres and thin films of nickel hydroxide and nickel oxide with hierarchical structures, J. Phys. Chem. B. 2005; 109(3) :1125–1129.

28. Z.H. Liang , Y.J. Zhu , X.L. Hu, β-Nickel hydroxide nanosheets and their thermal decomposition to nickel oxide nanosheets, J. Phys. Chem. B. 2004; 108(11): 3488–349.

29. J.H. Liang, Y.D. Li, Synthesis and Characterization of Ni(OH)$_2$ Single-crystal Nanorods, Chem. Lett. 2003; 32(12) : 1126–1127.

30. Z.Y. Wu, C.M. Liu, L. Guo, R. Hu, M.I. Abbas, T.D. Hu, H.B. Xu, Structural characterization of nickel oxide nanowires by X-ray absorption near-edge structure spectroscopy, J. Phys. Chem. B. 2005; 109(7): 2512–2515.

31. X.L. Li, J.F. Liu, Y.D. Li, Low-temperature conversion synthesis of M(OH)$_2$ (M=Ni, Co, Fe) nanoflakes and nanorods, Mater. Chem. Phys. 2003; 80(1): 222–227.

32. K. Nakamoto, Infrared and raman spectra of inorganic and coordination compounds, fifth ed., Wiley, New York, 1997.

33. P. Jeevanandam , Y. Koltypin , A. Gedanken, Synthesis of nanosized α-nickel hydroxide by a sonochemical method, Nano Lett. 2001; 1(5): 263–266.

34. G.J.D.A. Soler-Illia, M. Jobbagy, A.E. Regazzoni, M.A. Blesa, Synthesis of nickel hydroxide by homogeneous alkalinization, precipitation mechanism, Chem. Mater. 1999; 11(11): 3140–3146.

35. M.M. Kashani Motlagh, A.A. Youzbashi, F. Hashemzadeh, L. Sabaghzadeh, Structural properties of nickel hydroxide/ oxyhydroxide and oxide nanoparticles obtained by microwave-assisted oxidation technique, Powder Technol. 2013; 237: 562–568.

36. R.B. Viana, A.B.F. Dasilva, A.S. Pimentel, Infrared spectroscopy of anionic, cationic, and zwitterionic surfactants, Adv. Phys. Chem. 2012; 12: 2012.

37. S. Cabanas-Polo, K.S. Suslick, A.J. Sanchez-Herencia, Effect of reaction conditions on size and morphology of ultrasonically prepared Ni(OH)$_2$ powders, Ultrason. Sonochem. 2011; 18(4): 901–906.

38. S. Ren, C. Yang, C. Sun, Y. Hui, Z. Dong, J. Wang, X. Su, Novel NiO nanodisks and hollow nanodisks derived from Ni(OH)$_2$ nanostructures and their catalytic performance in epoxidation of styrene, Mater. Lett. 2012; 80: 23–25.